TECHNICAL REPORT STANDARD PAGE

1. Title and Subtitle
Analysis of Carbon Nanotube Reinforced Shape Memory Composites for Pavement Joints

2. Author(s)
Pengfei Zhang

3. Performing Organization Name and Address
College of Engineering
University of Louisiana at Lafayette
Lafayette, LA 70503

4. Sponsoring Agency Name and Address
Louisiana Department of Transportation and Development
P.O. Box 94245
Baton Rouge, LA 70804-9245

5. Report No.
FHWA/LA.17/001

6. Report Date
02/11/2021

7. Performing Organization Code
LTRC Project Number: 20-2TIRE
SIO Number: DOTLT1000299

8. Type of Report and Period Covered
Final Report
07/01/2019-12/31/2020

9. No. of Pages
37

10. Supplementary Notes
Conducted in Cooperation with the U.S. Department of Transportation, Federal Highway Administration

11. Distribution Statement
Unrestricted. This document is available through the National Technical Information Service, Springfield, VA 21161.

12. Key Words
Multi-walled CNT, self-healable polymer, shape memory recoverable polymer

13. Abstract
Joints exist in almost all manmade structures. Recycling of polymeric sealant has been explored in an attempt to reutilize materials. Several efforts have opted to address this subject from many perspectives including mechanical, chemical, and thermal recycling. Others have also delved into the self-healing/shape memory materials to remedy this dilemma. However, few studies have delved into understanding the role of carbon nanotube in self-healing/shape memory based recycled polymer composites. Therefore, in this study, experimental and simulation tools were utilized to understand the recycling process when CNTs were incorporated within recycled polycaprolactone/epoxy composites, which were developed for self-healing/shape memory purpose. A polynomial regression model, as a facile approach, was established to simulate the process-property relationship, which is essential for the successful implementation of the future of manufacturing. It found that, by adding CNTs, a reduction in the determined degree of crystallization was induced which correlated with the obtained reduction in the modulus and toughness. Strategies for enhancing mechanical properties have been pointed out for future endeavors.

Modeling and statistical understanding: the effect of CNT on mechanical properties of recycled polycaprolactone/epoxy composites

By
Pengfei Zhang
Co-principal Investigator

University of Louisiana at Lafayette
104 East University Avenue
Lafayette, LA 70503

LTRC Project No. 20-2TIRE
SIO No. DOTLT1000299

conducted for
Louisiana Department of Transportation and Development
Louisiana Transportation Research Center

022021

Abstract

Joints exist in almost all manmade structures. Recycling of polymeric sealant has been explored in an attempt to reutilize materials. Several efforts have opted to address this subject from many perspectives including mechanical, chemical, and thermal recycling. Others have also delved into the self-healing/shape memory materials to remedy this dilemma. However, few studies have delved into understanding the role of carbon nanotube in self-healing/shape memory based recycled polymer composites. Therefore, in this study, experimental and simulation tools were utilized to understand the recycling process when CNTs were incorporated within recycled polycaprolactone/epoxy composites, which were developed for self-healing/shape memory purpose. A polynomial regression model, as a facile approach, was established to simulate the process-property relationship, which is essential for the successful implementation of the future of manufacturing. It found that, by adding CNTs, a reduction in the determined degree of crystallization was induced which correlated with the obtained reduction in the modulus and toughness. Strategies for enhancing mechanical properties have been pointed out for future endeavors.

Acknowledgments

We gratefully acknowledge support from LTRC (DOTLT1000299).

Implementation Statement

The findings can be utilized by LADOTD for determining in-situ material properties and pavement joints.

Table of Contents

List of Tables

List of Figures

Introduction

Few studies have delved into understanding the role of carbon nanotube in self-healing/shape memory based recycled polymer composites. Thus, the focus in this study is to understand the recycling process when CNTs were incorporated within recycled polycaprolactone/epoxy composites, specifically the effect of the CNTs incorporation on the mechanical properties (elastic modulus and fracture toughness) of recycled PCL/Epoxy nanocomposites. A polynomial regression model, as a facile approach, was established to simulate the process-property relationship, which is essential for the successful implementation of the future of manufacturing. To further understand the impact of the CNTs inclusion into the polymer composite, nanoindentation, thermogravimetric analysis (TGA), differential scanning calorimetry (DSC), 3-point bending tests, Fourier-transform infrared spectroscopy (FTIR), and x-ray diffraction (XRD) were utilized to study the mechanical, thermal, and chemical behavior of the PCL/Epoxy/CNT composite. In order to produce a more compelling comparison, these analysis methods were conducted on 0%, 0.5%, and 1% CNT recycled polymer composites (percentages by weight).

Literature Review

With the advancements in polymer synthesis and development, many industries have opted to further expand their utilization of synthetic polymers. Thermoset and thermoplastic based synthetic polymers have been heavily utilized in industries including aerospace, consumer electronics, the automotive industries, and so on. To further improve the stiffness, strength-to-weight ratios, and the general mechanical and thermal properties of these polymers, reinforcing components such as carbon-based materials (e.g. carbon nanotubes (CNTs), carbon nanofibers (CNFs)) and cellulose have been incorporated into the polymers [1, 2]. Moreover, CNTs specifically have been extensively utilized due to their high aspect ratios, tensile strengths, etc. [3]. Much research has delved into the effects of incorporating these reinforcing materials on the mechanical, thermal, electrical, and chemical properties of several polymers (e.g. low-density polyethylene, poly-lactic acid, epoxies, poly-caprolactone (PCL), etc.). Moumen et al. conducted a study on three-phase materials consisting of epoxy, CNTs, and carbon fiber wherein it was reported that small concentrations of CNTs enhanced the elastic modulus, fracture toughness, and crack evolution resistance [4]. Qian et al. introduced a work focused on the dispersion of 1% MWCNTs within polystyrene which resulted in an average increase in elastic modulus of 39% [5]. Another study by Beircuk et al. incorporated 1% MWCNTs in epoxy with results obtained indicating a 125% improvement in thermal conductivity [6]. Several other contributions have also been done showing the extent to which research has been initiated in this area [7–10].

Unlike their thermoplastic counterparts, thermoset-based polymer composites cannot be remolded once formed due to the crosslinking that occurs between its constituent molecular chains [11]. This barrier has led to the research for the development of a recycling method for these materials. The need for such a method has been addressed from numerous perspectives including mechanical, chemical, thermal recycling, etc [12–14]. In the mechanical recycling perspective, grinding techniques are employed to reduce the polymer composite into fragments. From this point, the fiber- and polymer-rich fragments are separated with the polymer-rich components left nearly unusable. In thermal recycling, elevated temperatures are utilized to burn away the polymer matrix in order to recover the reinforcing material. As it can be seen here, both of these methods prioritize the recovery of the reinforcing material and thereby disregard the polymer components. Thus, these methods in their current form are not suitable for polymer recyclability. Chemical recycling on the other hand utilizes dissolution reagents that

cause the polymer matrix to undergo a degradation or depolymerization process [15–17]. In a work by Yu et al., thermosets capable of transesterification type bond exchange reactions were shown to be dissolvable in heated alcohol solvents (e.g. ethylene glycol) in approximately 3 hours and could then be repolymerized by heating [18]. Nevertheless, because the time necessary for chemical recycling can be very prolonged, it has yet to be widely applied for the recycling of polymer composites. One of the more interesting developments in this field is the utilization of self-healing materials to achieve polymer recyclability [19–21]. For instance, recyclable polymer composites based on self-healing effect were prepared through polymerization-induced phase separation [21]. The relationship between recycling process variables and material properties was studied by using response surface methodology (RSM) models. To our knowledge the effect of CNT incorporation on self-healing based recyclable polymer composites has been seldom studied.

It has been well-known that the RSM has a number of advantages on identifying inter-relationship between variables [21–23]. However, in order to obtain an optimal response, a sequence of designed experiments are highly required. For example, if the number of design variables is n, at least $2n + (2n + 1)$ sample groups are needed while using RSM central composite design (CCD) method. In other words, sample size becomes extremely large if the number of design variables is big, while using RSM model, which makes the experiment design complicated. It's been suggested that the number of major design variables could be reduced based on a rough assumption or experimental observations, and then the number of variables based on RSM model analysis could be further reduced [24]. However, such a to-and-fro process is much time consuming.

Objective

The focus in this study is to understand the recycling process when CNTs were incorporated within recycled polycaprolactone/epoxy composites, specifically the effect of the CNTs incorporation on the mechanical properties (elastic modulus and fracture toughness) of recycled PCL/Epoxy nanocomposites.

Methodology

- **Raw Materials and Preparation of Virgin Composite Sample**

Multi-walled carbon nanotube (Alfa Aesar Fullerene 95%, Fisher Scientific USA)with 0.1-10 μm in length, 1-3 nm and 3-20 nm in ID and OD, respectively. DPL 862 epoxy resin purchased from Applied Vehicle Technology, was utilized as the polymer matrix. Polycaprolactone (PCL) pellets, CAPA 6500, purchased from Perstorp were mixed with the epoxy resin material at a 3:22 volume ratio. This mixture was then cured with the triethylenetetramine (TETA) curing agent.

- **Preparation of Nanocomposites**

The samples tested in this work, were developed from a powder made using ball milling. In this milling process, the virgin material, shown in Figure 1, was first reduced to smaller shards and then crushed using a hydraulic platen press. After the completion of this step, the material was then milled into a fine powder using a Leeson ball miller. Sample sets with 0.5wt% and 1wt% MWCNTs were fabricated. The experiment variables were set as (x_1, x_2, x_3, x_4), i.e., (98,7,2,0), (98,7,2,0.5), (98,7,2,1), (98,7,0.15,0), (98,7,0.15,0.5), (98,7,0.15,1), (81,5,0.5,0), (81,5,0.5,0.5), (81,5,0.5,1), (114,9,0.5,0), (114,9,0.5,0.5), (114,9,0.5,1). Here x_1 is the mold temperature (oC), x_2 is the compressive pressure (MPa) to produce each sample, x_3 is the time (hr) for holding the applied pressure, and x_4 is the content of CNTs (weight by percent). The set values for x_1, x_2 and x_3 are suggested according to results from our previous work [21]. The sample preparation phase consisted of adding the CNT-incorporated milled powder to a mold and using an MTS Alliance RF/100 to supply the necessary compressive load to produce each sample (Figure 1). A furnace attached to the MTS allowed for precise temperature control while fabricating the samples. During this process, it was necessary to continuously monitor the compressive load to ensure it remained at the design value. However, once this load stabilized, a timer was set to control the compaction time. At the end of the compaction period, the furnace was opened allowing the sample to cool while the compressive force decreased to 0 N. At this point, the sample was removed from the machine and allowed to cool more prior to being removed from its mold.

Figure 1: Steps performed in the sample preparation process [25]

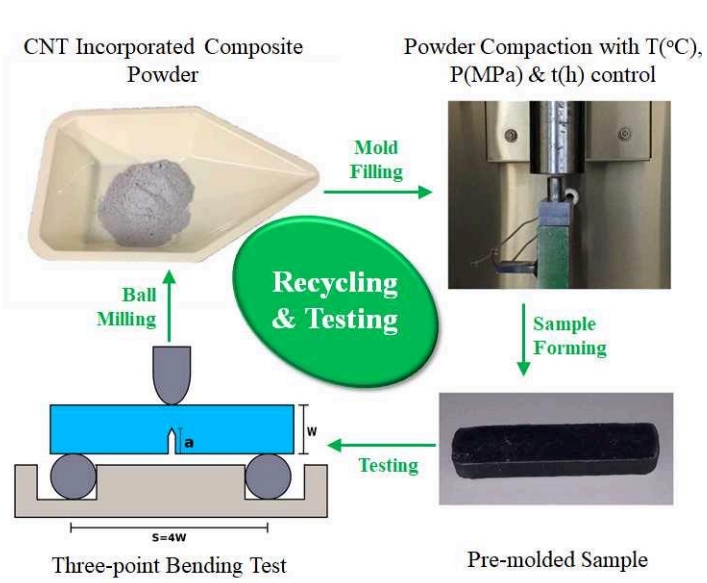

- **Characterization**

An FTIR analysis was conducted upon the PCL/Epoxy nanocomposite. To ascertain the effect of the incorporation of MWCNTs on the PCL/Epoxy nanocomposite, such as the degree of crystallization, a PerkinElmer DSC4000 was employed with the tests conducted under a heating, cooling, and isothermal procedure. Furthermore, a TGA1000 was employed to determine the nanofillers effect on the thermal stability of the polymer nanocomposite. A Hitachi S3000 scanning electron microscope (SEM) was used to obtain micrographs of the fracture surfaces of the polymer nanocomposite. The fabricated specimens were gold sputter-coated up to 15 nm thickness. An accelerating voltage of 25 kV was applied to obtain micrographs of the desired magnification. To gain an understanding of the effect of the addition of MWCNTs into the polymer nanocomposite, a Rigaku MiniFlex 600 X-ray Diffractometer was employed to perform powder diffraction analysis on the pure epoxy and pure (i.e., 0wt%), 0.5wt%, and 1wt% CNT recycled polymer composites.

Nanoindenter XP G200 from Agilent Instruments equipped with a three-sided Berkovich pyramidal diamond tip was used in this study to measure mechanical properties of the polymer composites at micro level. The nanoindentation (NI) experiments were conducted at room temperature using continuous stiffness measurement (CSM) method at maximum depth of 10 µm. The harmonic displacement of the sinusoidal load was set as 2 nm with a 45 Hz frequency and the strain rate was chosen as 0.05 s^{-1}. In order to avoid

the effect of tip blunting on the calculated NI results, tip area calibration was performed by conducting 25 indentations on a reference fused silica sample (with E = 72 GPa). For all measurements, 25 indentations were conducted in a grid of 5×5 points with a minimum spacing of 200 μm between adjacent indents to avoid any interactions between the plastic regions.

To quantitively measure the effect of the CNT reinforcement on the mechanical properties of the recycled PCL/epoxy nanocomposites, 3-point bending tests were performed. This test was conducted in reference to the ASTM D5045 standard which details a method for calculating a critical-stress-intensity factor. This was done by first creating a pre-crack in the samples such that the crack length to specimen width ratio was approximately 0.45-0.50 as shown in Figure 1. Each sample set consisted of three specimens which were cut using a precision saw to the required dimensions as outlined in ASTM D5045. The specimen, now with its pre-crack, was placed in the 3-point bending fixture with a span of 41 mm and a loading rate of 10 mm/min (Figure 1). From the load vs strain curve produced and the calculated geometric factor from the aforementioned standard, the critical-stress-intensity factor was determined for each specimen. This critical-stress-intensity factor (K_Q) was calculated using Equations 1 and 2 shown below wherein P_Q is the peak load (kN), B is the specimen thickness (cm), W is the specimen width (cm), a is the crack length (cm), and x is the ratio of a to W

$$K_Q = \frac{P_Q}{BW^{0.5}} f(x) \quad (1)$$

$$f(x) = 6\sqrt{x}\,\frac{1.99 - x(1-x)(2.15 - 3.93x + 2.7x^2)}{(1+2x)(1-x)^{1.5}} \quad (2)$$

- **Polynomial Regression Process**

The process of regression was implemented by R program, which is a free, open source software environment for statistical computing and graphics. It compiles and runs on a wide variety of UNIX platforms, Windows and MacOS. Because none of the variables meet the requirements of the normality, the analysis of variance (ANOVA) is not an appropriate way to fit the data. Thus regression model was considered in this study. We used different criteria to judge the fitting effect of the model, including the significant levels of the predictor variables, the coefficient of multiple determination (R^2), and the adjusted coefficient of multiple determination (AdjustedR^2). In this study, we used the p-value to judge the significant level of the variable, i.e., the smaller the p-value is, the more significance the variable is. As mentioned above, x_1, x_2, x_3 and x_4 represent four

predictor variables, which are temperature (^{o}C), pressure (MPa), time (hr) and the amount of CNT (weight by percent). The response variable is y (critical-stressintensity factor, MP a.m$^{0.5}$). We then ran a residual analysis by performing test of normality, test of outliers, and test for homogeneity of variance. The results show that the computed residuals meet all the assumptions and illustrate good asymptotic properties.

Discussion of Results

- **Molecular Structure and Its Bonding**

FT-IR results show that the primary and subsequent traces possess nearly, if not exactly, the same wavenumbers, as shown in Figure 2a. The similarity between these analyses indicates no changes in bonds and functional groups before and after the preparation of polymer composites. In Figure 2b, it shows XRD diffraction curves obtained for the pure epoxy and the pure (0 wt% CNT), 0.5 wt% CNT, and 1 wt% CNT polymer composites. The main component is the crosslinked DPL 862 resin for pure epoxy. And it consists of crosslinked 862 resin and PCL phase for pure polymer composites. For 0.5 wt% CNT and 1 wt% CNT polymer composites, they have three components, which are crosslinked DPL 862 resin, PCL, and CNT. Its been well known that the incorporation of CNT in a polymer composite would definitely affect its mechanical property, either property improvement or deterioration. The XRD is a good tool to understand how CNT can affect its mechanical properties from the perspective of crystal structure change. From the plot, the curve for pure epoxy contains both k-alpha1 and k-alpha2 radiation at angles of 19.90^{o} and 23.36^{o} on (100) planes, respectively. The 2-theta degree of k-alpha1 has been shifted to 21.28^{o} for all composite samples. On (110) planes, the curves for pure epoxy and pure polymer composite samples have k-alpha1 and k-alpha2 at 29.35^{o} and 30.65^{o}, respectively. But the k-alpha2 disapears for CNT incorporated composite samples. The disappearance of k-alpha2 at 30.65^{o} does not suggest there is any change in the crystalline structure; instead, it might be attributed to a more compact structure after the incorporation of CNT within composite samples [26]. It also shows that the curves remain same for all samples on (111) and (200) planes.

Figure 2: Comparison using (a) FTIR and (b) XRD diffraction [25]

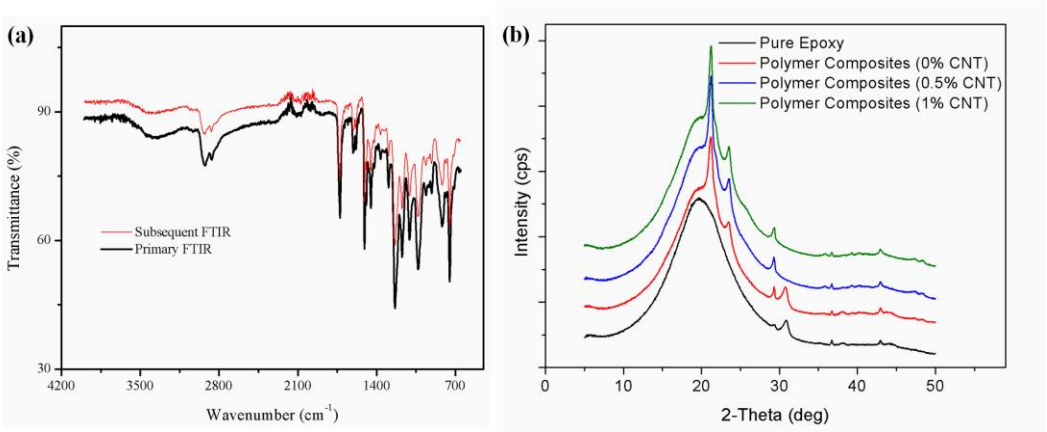

Using the analysis software provided with the Rigaku MiniFlex 600, the degree of crystallization was determined for each sample, as shown in Table 1. From the table one can see that the addition of the PCL component to the epoxy resulted in an increase of the crystallinity from approximately 4.13% to 16.8%. This is because of the plasticization effect of PCL [27, 28]. However, it was noted that the addition of CNTs resulted in the reduction of the crystallinity to 14.5% for the 0.5 wt% CNT and and 12.0% for the 1 wt% CNT polymer composites. It shows there is a change but with a slight difference. As mentioned earlier, the incorporation of CNT would not change the crystalline structure. But the aggregation of CNT would affect the self-nucleation rate of PCL [29]. Therefore, the degree of crystallization would be affected if CNT is not well-dispersed within composite samples.

Table 1: X-Ray Diffraction Crystallinity of samples [25]

Sample	**Degree of Crystallization (%)**
Pure Epoxy	4.13
Polymer Composite	16.8
0.5% CNT Polymer Composite	14.5
1% CNT Polymer Composite	12.0

- **Elastic Modulus**

According to the above discussion, it is rational to assume that only three phases exist (CNT, epoxy particles, and PCL) within the nanocomposites. The CNT and PCL are perfectly bonded to each other in a physical manner; so are the epoxy particles and PCL. Figure 3 schematically shows the RVE of CNT incorporated PCL/epoxy composites. The Mori-Tanaka micromechanical model was used to predict the elastic properties [30–32]. In this study, the overall elastic-stiffness tensor **C** of the composite is

$$C = \Pi + \Gamma \tag{3}$$

where the boldface terms indicate tensor quantities, Π and Γ are the stiffness tensors of the epoxy/PCL and CNT/PCL parts, respectively. For the epoxy/PCL part, the elastic stiffness tensor is

$$\mathbf{\Pi} = (\forall^P \boldsymbol{C}^P + \forall^E \boldsymbol{C}^E \boldsymbol{T}^E)(\forall^P \boldsymbol{I} + \forall^E \boldsymbol{T}^E)^{-1} \tag{4}$$

where $\forall^E$ and $\forall^P$ are the effective volume fractions of epoxy and PCL phases, respectively; $\boldsymbol{I}$ is the identiy tensor; $\boldsymbol{C^E}$ and $\boldsymbol{C^P}$ are the stiffness tensors of the effect epoxy

and PCL, respectively. It is assumed the individual epoxy particle and PCL phase are isotropic materials, expressed as

$$\left[C^n\right] = \begin{bmatrix} \frac{1}{E^n} & -\frac{\nu^n}{E^n} & -\frac{\nu^n}{E^n} & 0 & 0 & 0 \\ -\frac{\nu^n}{E^n} & \frac{1}{E^n} & -\frac{\nu^n}{E^n} & 0 & 0 & 0 \\ -\frac{\nu^n}{E^n} & -\frac{\nu^n}{E^n} & \frac{1}{E^n} & 0 & 0 & 0 \\ 0 & 0 & 0 & \frac{2(1+\nu^n)}{E^n} & 0 & 0 \\ 0 & 0 & 0 & 0 & \frac{2(1+\nu^n)}{E^n} & 0 \\ 0 & 0 & 0 & 0 & 0 & \frac{2(1+\nu^n)}{E^n} \end{bmatrix}$$

where ***n*** represents epoxy or PCL phase, and $\boldsymbol{E^n}$ represents the isotropic Young's modulus. The $\boldsymbol{T^E}$ is the dilute strain-concentration tensor of the effective particles, which is given by

$$\boldsymbol{T}^E = [\boldsymbol{I} + \boldsymbol{S}^E(\boldsymbol{C}^P)^{-1}(\boldsymbol{C}^E - \boldsymbol{C}^P)]^{-1} \tag{5}$$

where $\boldsymbol{S^E}$ is the Eshelby tensor for spherical effective epoxy particle and an isotropic PCL phase. The components of the Eshelby tensor are

$$\begin{aligned} S_{1111} = S_{2222} = S_{3333} &= \frac{7-5\nu}{15(1-\nu)} \\ S_{1122} = S_{2233} = S_{3311} = S_{1133} = S_{2211} = S_{3322} &= \frac{5\nu-1}{15(1-\nu)} \\ S_{1212} = S_{2323} = S_{3131} &= \frac{4-5\nu}{15(1-\nu)} \end{aligned} \tag{6}$$

where ***v*** is the Poisson's ratio of the PCL phase. By implementing Eqs.(5) & (6) into Eq.(4), it leads to the calculation of stiffness tensor for epoxy/PCL part.

Figure 3: Representative volume element (RVE) of CNT incorporated PCL/epoxy composite that consists of three constituents: CNT, epoxy particles, and PCL [25]

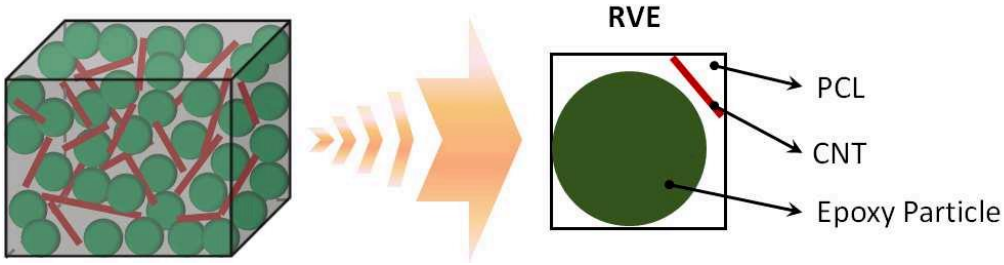

For the CNT/PCL part, the transversely isotropic inclusion is treated as a solid cylinder so to neglect the hollow nature of CNT [31]. The specific form of CNT is neglected as well. What's more, any possible relative motion between individual nanotubes in a CNT bundle is not taken into account. Thus the elastic stiffness tensor is given as

$$\boldsymbol{\Gamma} = \boldsymbol{C}^P + \forall^T \langle (\boldsymbol{C}^T - \boldsymbol{C}^P)\boldsymbol{A}^T \rangle [(1-\forall^T)\boldsymbol{I} + \forall^T \langle \boldsymbol{A}^T \rangle]^{-1} \tag{7}$$

where $\forall^T$ is the CNT volume fraction; $\boldsymbol{I}$ is the identity tensor; $\boldsymbol{C^T}$ is the stiffness tensors of the CNT, which is assumed to be transversely isotropic material, as

$$\left[C^T\right] = \begin{bmatrix} \frac{1}{E_1} & -\frac{\nu_{12}}{E_1} & -\frac{\nu_{12}}{E_1} & 0 & 0 & 0 \\ -\frac{\nu_{12}}{E_1} & \frac{1}{E_2} & -\frac{\nu_{23}}{E_2} & 0 & 0 & 0 \\ -\frac{\nu_{12}}{E_1} & -\frac{\nu_{23}}{E_2} & \frac{1}{E_2} & 0 & 0 & 0 \\ 0 & 0 & 0 & \frac{2(1+\nu_{23})}{E_2} & 0 & 0 \\ 0 & 0 & 0 & 0 & \frac{1}{G_{12}} & 0 \\ 0 & 0 & 0 & 0 & 0 & \frac{1}{G_{12}} \end{bmatrix}$$

From the five independent elastic moduli (i.e., E_1, ν_{12}, G_{12}, K_{23}, and G_{23}), the other elastic component are given as [33]

$$E_2 = \frac{4G_{23}K_{23}}{K_{23} + \psi G_{23}}$$
$$\nu_{23} = \frac{K_{23} - \psi G_{23}}{K_{23} + \psi G_{23}}$$
$$\psi = 1 + \frac{4K_{23}{\nu_{21}}^2}{E_1} \tag{8}$$

And $\mathbf{A^T}$ is the dilute mechanical strain concentration tensor for the CNT phase, given as

$$\boldsymbol{A}^T = [\boldsymbol{I} + \boldsymbol{S}^T(\boldsymbol{C}^P)^{-1}(\boldsymbol{C}^T - \boldsymbol{C}^P)]^{-1} \tag{9}$$

where the terms enclosed in brackets in Eq.(9) represent the average of the term over all orientations defined by the transformation from the local carbon nanotube coordinates to the global composite coordinate system; $\boldsymbol{S^T}$ is Eshelby's tensor representing the high aspect ratio (length/diameter) of CNT and an isotropic PCL phase [34, 35]

$$
\begin{aligned}
S_{2222} = S_{3333} &= \frac{5-4\nu}{8(1-\nu)} \\
S_{2211} = S_{3311} &= \frac{\nu}{2(1-\nu)} \\
S_{2233} = S_{3322} &= \frac{4\nu-1}{8(1-\nu)} \\
S_{1212} = S_{1313} &= \frac{1}{4} \\
S_{2323} &= \frac{3-4\nu}{8(1-\nu)}
\end{aligned} \tag{10}
$$

Likewise, the implementation of Eqs.(8)&(9) & (10) into Eq.(7) leads to the determination of stiffness tensor for CNT/PCL part. Thus the overall elastic-stiffness tensor can be calculated by Eq.(3).

The sample elastic modulus was measured at small scale by CSM based NI technique, which uses a superimposed oscillatory load on top of the main motion driving force to record elastic modulus as a function of penetration depth. Throughout the indentation loading segments, a polynomial approximation of the tip geometry was calculated based on the calibration experiments to take into account of the tip geometry imperfections from its pyramidal shape, and further to find an optimum penetration depth beyond which the measured properties are stable [36, 37]. It is suggested that the elastic modulus, according to the Oliver-Pharr method, could be derived analytically in terms of overall elastic-stiffness tensor components as [38–40]

$$
M_a = 2\sqrt{\frac{C_{11}C_{33}-C_{13}^2}{C_{11}}\left(\frac{1}{C_{44}}+\frac{2}{\sqrt{C_{11}C_{33}}+C_{13}}\right)^{-1}} \tag{11}
$$

$$
M_t = \sqrt{\frac{C_{11}^2-C_{12}^2}{C_{11}}\sqrt{\frac{C_{11}}{C_{33}}}M_a} \tag{12}
$$

where $\boldsymbol{M_a}$ and $\boldsymbol{M_t}$ are indentation modulus under the axial and transverse indent, respectively. The calculated indentation modulus are for materials that are linear elastic and symmetrical in response to mechanical tests when a conical indenter is used. In this study, the indentation modulus $\boldsymbol{M_t}$ represents the elastic modulus of composite sample.

For the micromechanical model, in order to calculate the elastic modulus, following parameters are used: (1) For isotropic compliance of PCL, $\boldsymbol{E^{PCL}}$=0.28 GPa, $\boldsymbol{v^{PCL}}$=0.3; (2) For isotropic compliance of epoxy, $\boldsymbol{E^{epoxy}}$=3.5 GPa, $\boldsymbol{v^{epoxy}}$=0.33; (3) For transversely isotropic stiffness of CNT, $\boldsymbol{E^{1}}$=905 GPa, $\boldsymbol{v^{12}}$=0.163, $\boldsymbol{G^{12}}$=240 GPa, $\boldsymbol{K^{23}}$=210 GPa, $\boldsymbol{G^{23}}$=80 GPa; (4) For sample with 0 wt% CNT, volume fractions, $\forall^E$=0.88, $\forall^P$ =0.12; (5) For

sample with 0.5wt% CNT, volume fractions, $\forall^E$=0.8773, $\forall^P$ =0.1196, $\forall^T$ =0.0031; (6) For sample with 1 wt% CNT, volume fractions $\forall^E$=0.8746, $\forall^P$ =0.1193, $\forall^T$ =0.0061; (7) To determine the above volume fractions, densities of epoxy/PCL/multi-wall CNT are $\boldsymbol{\rho}^{epoxy}$=1.11 g/cm^3, $\boldsymbol{\rho}^{PCL}$=1.12 g/cm^3, $\boldsymbol{\rho}^{CNT}$ =1.89 g/cm^3. Figure 4 shows a depiction of the determined elastic modulus, both from model prediction and experimental nanoindentation tests, for the pure (0 wt%), 0.5 wt%, and 1 wt% CNT polymer composites fabricated under the experiment design conditions. According to the micromechanical model, the trend of the increase in elastic modulus indicates that there is a critical point on the curve, suggesting continuously loading CNT would not improve the elastic modulus. Determination of the critical point is not the interest in this study.

Figure 4: Elastic modulus from model prediction and nanoindentation tests [25]

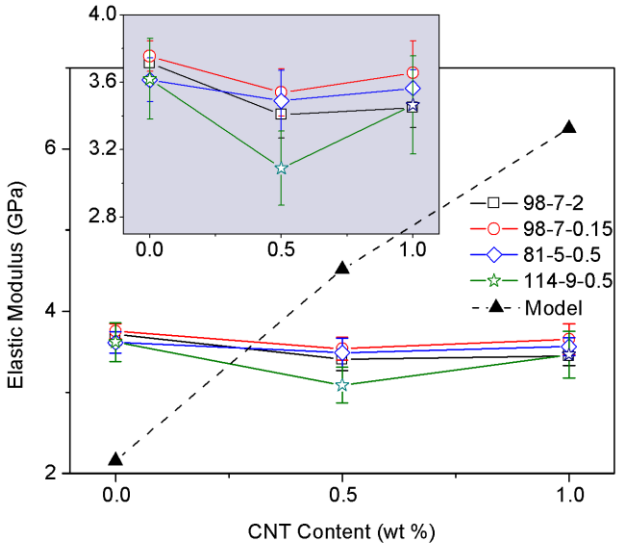

Compared with the model prediction, the measured elastic modulus are smaller for samples with CNT but larger for sample without CNT. It is worthy noting that, in this study, the effect of particle size was not considered in this micromechanical model. As suggested by Fu et al, the Young's modulus of particulate polymer composites would be affected by particle size if the particle volume fraction is above 18% [41]. The epoxy particle volume fraction here is no less than 80%. According to Figure 5, the particle sizes are only a few micrometers. The larger measured modulus for samples without CNT might be attributed to the coupling effect of epoxy particle sizes.

Figure 5: Micrograph obtained for recycled polymer composite at X600 [25]

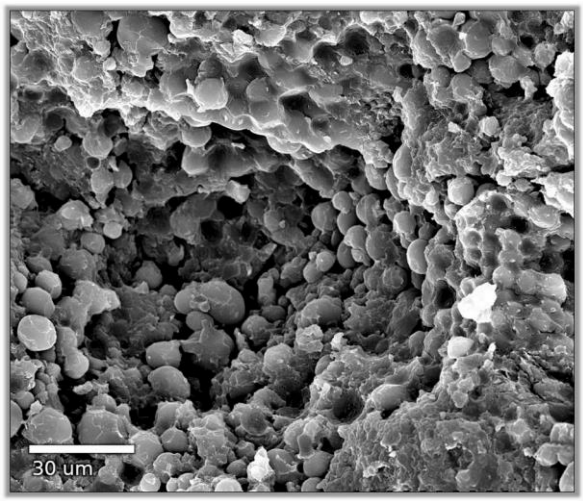

Accoding to the nanoindentation measurement, the CNT incorporated samples possessed a lower modulus than pure composite sample. But when increasing the CNT content from 0.5 wt% to 1 wt%, there is an improvement in the modulus. And there is a trend indicating an increase in modulus along with CNT adding. Such result agrees with the degree of crystallinity (see Table 1). However, the measured elastic modulus for samples with multi-walled CNT are below the predicted modulus. Keep in mind, assumption of the model in this study is that all three phases are perfectly bonded to each other in a physical manner. However, through morphology characterization, there are defects within samples. For instance, in Figure 5, one can see that the composite is composed of several spherically shaped structures, which are epoxy cores encapsulated by a PCL coating [21]. In Figures 6A and 7A, there were areas with what appeared to be specks in the 0.5 wt% and 1 wt% CNT incorporated PCL/epoxy nanocomposites. These specks were the CNTs. Moreover, it was noted that the CNTs seemed to have agglomerated into small areas within the micrograph. In the 1wt% CNT micrographs, the agglomerated areas were smaller in size and better dispersed in comparison to the 0.5 wt% CNT micrograph, which depicted one very large area filled with CNTs. It is clear to see that, from Figures 6C, 6D, 7C, and 7D, the shear disparity in the dispersion such that some areas were nearly or absolutely free of any of the CNTs. In short, the introducing of CNTs into recycled PCL/epoxy composites has resulted in internal defects within samples. The physical interphase bonding is no longer perfect, leading to a reduction of elastic modulus in CNT incorporated recycled PCL/epoxy composites.

Figure 6: Micrographs obtained for 0.5% CNT incorporated recycled PCL/epoxy polymer composite taken at magnifications of X500 (A), X1500 (B), X1500 (C), and X4500 (D) [25]

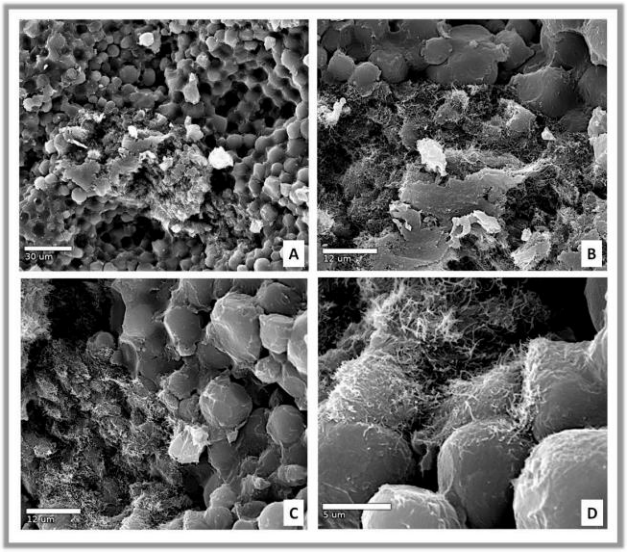

Figure 7: Micrographs obtained for 1% CNT incorporated recycled PCL/epoxy polymer composite taken at magnifications of X500 (A), X1500 (B), X2000 (C) and X4000 (D) [25]

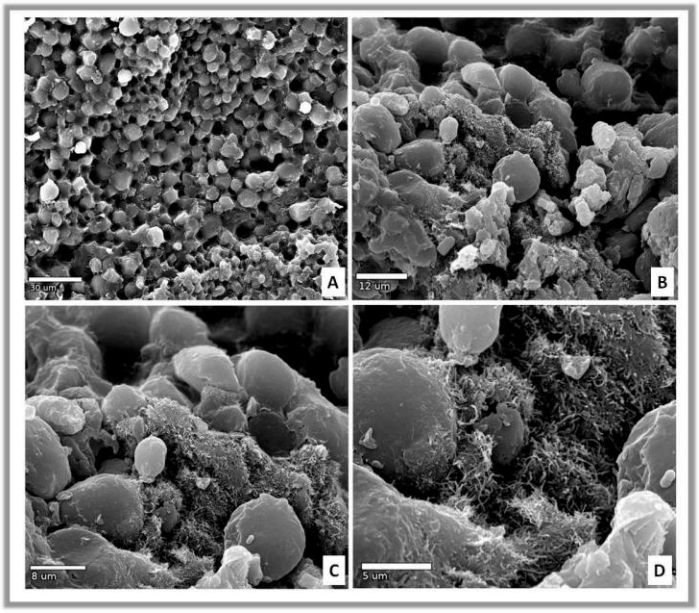

- **Flexural Behavior**

As a means of ascertaining the effect of the CNT reinforcement on the recycled PCL/Epoxy composite system, 3-point bending tests were performed in accordance to

ASTM D5045. Figure 8 depicts typical load-displacement curves obtained from 3-point bending tests for the pure (i.e., 0wt%), 0.5wt%, and 1wt% CNT recycled polymer composites in comparison to that of the virgin polymer composite. Using the data collected from flexural tests, the critical-stress intensity factors were calculated for those sample sets using Eqs. (1) and (2).

Figure 8: Typical 3-point testing result for the comparison obtained from the virgin and recycled polymer composites (i.e. pure, 0.5% CNT, and 1% CNT) [25]

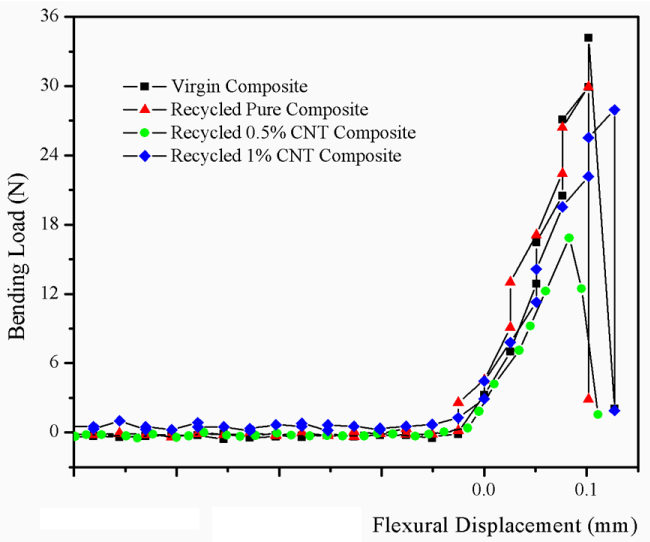

Unlike the micromechanical model built for elastic modulus, the energy concept of linear elastic fracture mechanics is applied in this case to understand the fracture behavior. Similar to Griffith criterion, fracture occurs at a stress that corresponds to a critical value of the strain energy release rate. For plane strain, the critical stress $\boldsymbol{\sigma_c}$ at fracture is

$$\sigma_c = \sqrt{\frac{E_n G_c}{\pi a(1-\nu^2)}} \tag{13}$$

where $\boldsymbol{E_n}$ is the Young's modulus of CNT incorporated PCL/epoxy nanocomposites, $\boldsymbol{\nu}$ is the Poisson's ratio of nanocomposites, $\boldsymbol{G_c}$ is the strain energy release rate, $\boldsymbol{a}$ is the crack length. Since single-edge notched specimens were tested in this study, the energy release rate $\boldsymbol{G_c}$ must be equal to the energy necessary $\boldsymbol{R_{ii}}$ (crack resistance) to initiate crack propagation [42], which gives

$$G_C = R_{ii}(i = p, t) \tag{14}$$

where $\boldsymbol{R_{pp}}$ represents the energy necessary between epoxy particles, $\boldsymbol{R_{tt}}$ represents the energy necessary between MWNTs. Due to the scale effect, the energy necessary between

epoxy particle and MWNT could be ignored. As explained in Figure 3, all epoxy particles and CNTs are bonded by PCL phase. But, as shown in Figures 6D and 7D, debonding of particles from a surrounding matrix is dominant. The bonding strength at the particle/matrix interface is much weak. Herein debonding starts before nano-matrix phase yielding. Figure 9 shows the situation of the dissipation and process zones under static loading. According to above discussion, the nanocomposite adhesive layer consists of PCL and CNT. Following the energy debonding criterion, for the case $R_{pp} \ll R_{tt}$, the critical-stress-intensity factor is determined as

$$K_{IC} = \sqrt{\frac{E_n \boldsymbol{R_{pp}}}{1-\nu^2}} \tag{15}$$

As suggested, using both the critical strain criterion and the energy criterion of debonding, the energy necessary between particles is

$$\boldsymbol{R_{pp}} = \frac{2\gamma_m \alpha^{-2}(\zeta)}{1 - \frac{2\beta(\chi)}{E_n}(1.5E_m(\chi)(1+\nu_m)\zeta\alpha^2(\zeta) + \frac{\alpha(\zeta)\omega_m(\chi)}{(1-\zeta)(\epsilon_{my}(\chi))^2})} \tag{16}$$

where $\boldsymbol{\gamma_m}$ is the local specific fracture energy of the nanocomposite adhesive; $\boldsymbol{\chi}$ is the weight percentage of CNT; $\omega_m(\chi)$ is the volume specific plastic energy of the adhesive; $\boldsymbol{E_m(\chi)}$ and $\boldsymbol{\nu_m}$ are the modulus and Poisson's ratio of the adhesive (it is assumed here that the change of Poisson's ratio along with amount of CNT is ignored); $\boldsymbol{\varepsilon_{my}(\chi)}$ is the yield strain of the adhesive layer under the mode I fracture [43]; $\boldsymbol{\beta(\chi)}$ is the fitting parameter given as $\boldsymbol{\beta}(\chi) = 0.022\chi^2 - 0.023\chi + 0.027$; ζ is the particle volume fraction; the strain concentration factor α is given as $\boldsymbol{\alpha(\zeta)} = (1-\zeta)^{-1}$.

Figure 9: Dissipation and process zones in front of a crack and the interaction between epoxy particles [25]

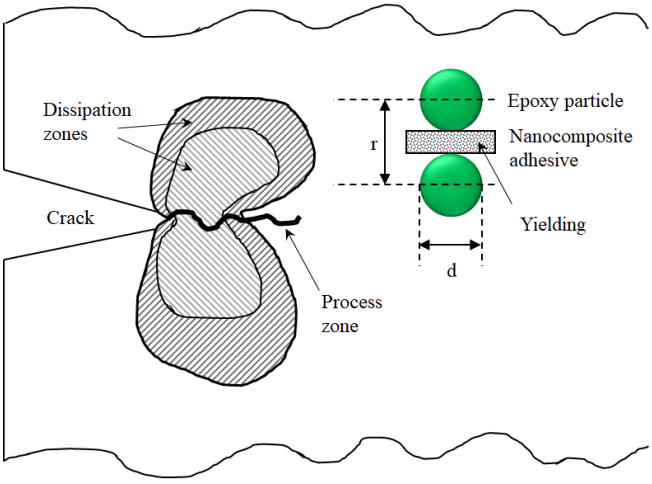

In order to calculate the predicted critical-stress-intensity factors, following parameters are used: (1) The local specific fracture energy of the nanocomposite adhesive layer is 370 J/m^2; (2) Weight percentage of CNT: χ = 0 wt%, 0.5 wt%, and 1.0 wt%; (3) Volume fraction of epoxy particles: ζ = 0.88, 0.8773, and 0.8746 for the case of 0 wt%, 0.5 wt%, and 1.0 wt%, respectively; (4) To obtain the Young's modulus of adhesive layer, PCL/CNT samples were prepared for tensile test, according to the stress-strain curves, following results were determined as: $\mathbf{E_m(0)}$ = 385 MPa, $\mathbf{E_m(0.5)}$ = 350 MPa, and $\mathbf{E_m(1.0)}$ = 348 MPa; $\boldsymbol{\varepsilon_{my}(0)}$ = 0.06, $\boldsymbol{\varepsilon_{my}(0.5)}$ = 0.04, and $\boldsymbol{\varepsilon_{my}(1.0)}$ = 0.04; $\boldsymbol{\omega_m(0)}$ = 0.48 MPa, $\boldsymbol{\omega_m(0.5)}$ = 0.274 MPa, and $\boldsymbol{\omega_m(1.0)}$ = 0.272 MPa; $\boldsymbol{\nu_m}$ = 0.3; (5) Strain concentration factor: $\boldsymbol{\alpha(0.88)}$ = 8.33, $\boldsymbol{\alpha(0.8773)}$ = 8.15, and $\boldsymbol{\alpha(0.8746)}$ = 7.97; (6) Fitting parameter: $\boldsymbol{\beta(0)}$ = 0.027, $\boldsymbol{\beta(0.5)}$ = 0.021, and $\boldsymbol{\beta(1.0)}$ = 0.026. Figure 10 shows a depiction of the determined critical-stress-intensity factor, both from model prediction and 3-point bending tests, for the pure (0 wt%), 0.5 wt%, and 1 wt% CNT polymer composites. The K_Q values of the CNT incorporated recycled polymer composites are lower than that of the pure recycled composite. More specifically, one can see that the 0.5wt% CNT composites produced quantities lower than the 1wt% CNT composites. To this point, it shows the reduction in the crystallinity agreed with the reduction observed in the critical-stress-intensity factor and elastic modulus.

Figure 10: Comparison of the measured and predicted critical-stress-intensity factor obtained for the samples (i.e. pure, 0.5% CNT, and 1% CNT) [25]

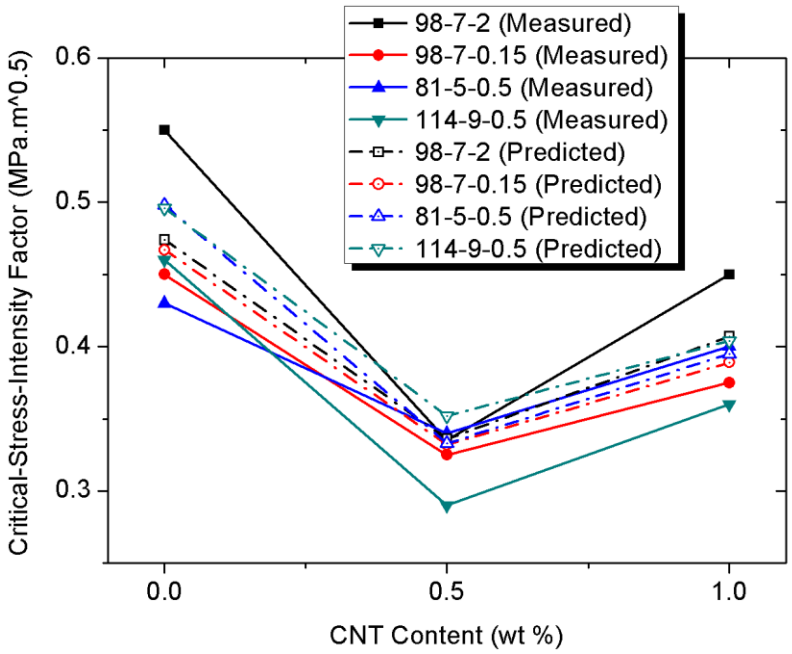

- **Regression Analysis of Flexural Behavior**

The regression analysis was constructed as follows. The coefficient of correlation of the response and predictor variables was checked firstly. The value range of the coefficient is from -1 to +1. A positive or negative sign means there is either a positive linear relationship or negative linear relationship between variables. A coefficent which is close to -1 or +1 indicates there is a strong linear relationship. On the other hand, a near zero means there is no significant relationship. The result is illustrated in Table 2, from which it can be seen that x_1 and x_2 are highly correlated. But do neither of these two predictor variables have a strong relation with the response variable y. It can also be seen that both predictor variable x_3 and x_4 are highly correlated to the response variable y. Then we performed a linear regression with the original data set. The result indicates that the data in their original form can not explain the relationship between predictor and response variables very well. We raised the dimension number of the data from 4 to 42 to fit a polynomial regression, by adding interactive items, quadratic terms, cubic terms, logarithmic transformation, and exponential transformation. After running the regression, we got a model with (R^2 = 0.9199 and the AdjustedR^2 = 0.8899), which fits the data pretty well. The results are shown in Table 3, from which we can see that the Intercept, x_3, x_4 and x_4^2 are significant, so they all should be involved in our model. The model can be written as

$$y = 0.446748 + 0.038098x_3 - 0.5235x_4 + 0.442x_4^2 \quad (17)$$

Table 2: Coefficient of variable correlation [25]

	x_1	x_2	x_3	x_4	y
x_1	**1**	**0.99977**	**0.00862**	**0**	**-0.075398**
x_2	**0.99977**	**1**	**0**	**0**	**-0.080334**
x_3	**0.00862**	**0**	**1**	**0**	**0.386558**
x_4	**0**	**0**	**0**	**1**	**-0.472507**
y	**-0.075398**	**-0.080334**	**0.386558**	**-0.472507**	**1**

The model which fitted by 12 sets of data performs well in statistics, as shown in the Figure 11. The values appear to generally follow a straight line. It can be seen that

majority points are on the line or close to the line, which proves good matching of model and experiment. With the comparison, the accuracy of the polynomial model is considerable good.

Table 3: Level of significance for the predictors [25]

	Coefficients	P-value	Level of Significance
Intercept	**0.446748**	**1.31e-09**	**Very significant**
x_3	**0.038098**	**0.00479**	**Significant**
x_4	**-0.5235**	**3.03e-05**	**Very significant**
x_4^2	**0.442**	**7.67e-05**	**Very significant**

Figure 11: Predicted and measured K_Q from fitted model and experimental tests [25]

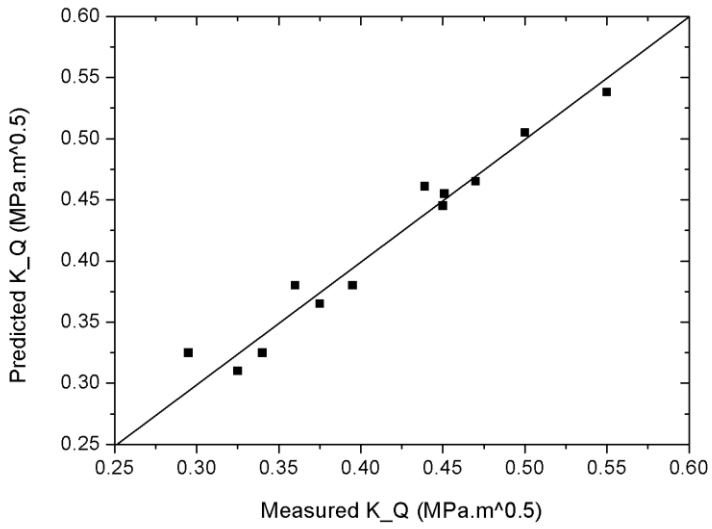

We then perform a residual analysis, which includes test of normality, outliers, and homogeneity of variance. To test the normality, we performed a shapirio-wilk test. The p-value of the test is 0.1509, which indicates the residuals are from a normal population. To check the existence of the outliers, we used Dixon.test from outliers package in R program. The p-value of the test is 0.1614, so there is not enough evidence to support if there is any outliers. We then performed a test for homogeneity of variance by using ncvTest function in R program, the resulting p-value 0.77902 indicates a strong evidence

of the homogeneity of variance. Keep in mind, the experiment was conducted at 81°C, 98°C, and 114°C. As can be seen from Figure 12, there is no obvious trend in the influence of temperature on K_Q. At 98°C, the maximum K_Q appeared. The pressure values were 5 MPa, 7 MPa, and 9 MPa, respectively. The maximum K_Q in the dataset appeared when pressure was 7 MPa. There is a trend suggesting that the K_Q increases with the pressure holding time. As the amount of CNT increases, the K_Q first decreases and then increases. The maximum K_Q occurs when the amount of CNT is 0. So it suggests that, in the future recycling, we can safely choose arbitrary levels of temperature and pressure as long as they are acceptable. More attention must be put on the setups of the compact time and the CNT amount.

Figure 12: Influence of temperature, pressure, time and CNT amount on K_Q [25]

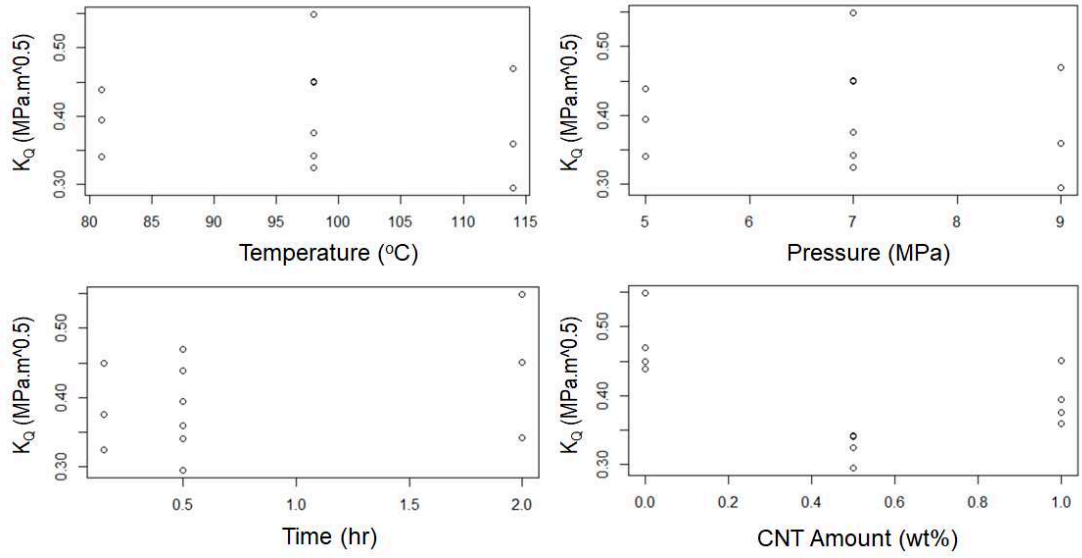

Conclusions

In this project, the effect of MWCNTs reinforcement on the mechanical properties of a recycled self-healable/shape memory PCL/Epoxy polymer composite was studied. Through the application of the sample preparation processes, nanocomposite samples were fabricated and characterized via several testing methods and morphological analyses. Mori-Tanaka micromechanical model was established for predicting elastic modulus of the CNT incorporated recycled PCL/epoxy nanocomposites. A general problem in the micromechanical modelling is the determination of realistic input parameters, especially in the case of having intrinsic defects due to the processing. A model based on linear elastic fracture mechanics was selected to predict the flexural properties of the nanocomposites. A polynomial regression model was generated to simulate the process-property relationship. It suggests the future effort on preparing recycled PCL/epoxy nanocomposites with high performance should be put on the processing compact time and the amount of CNTs.

From the obtained SEM micrographs, it was clear that there was a poor dispersion of CNTs in the 0.5wt% and 1wt% CNT composites and was more pronounced in the 0.5wt% CNT sample. In the analysis performed on the nanoindentation and flexural tests results, it was evident that the elastic modulus and K_Q of the CNT infused composites was reduced in comparison to the pure recycled composite. Moreover, it was found that the 1wt% CNT composites possessed higher properties in comparison to the 0.5% composites. Similar results were discovered in the determined degree of crystallization such that the pure recycled composite possessed a higher crystallinity than the 0.5wt% CNT and 1wt% CNT recycled composites. Therefore, from the results obtained from the analyses and micrographs, it was concluded that the lack of significant improvement in the K_Q and general thermal and mechanical properties with CNT incorporation as expected was due in part to the epoxy phase within the material and the poor dispersion of the nanomaterials in the composite. This is because the level of CNT dispersion plays a vital role in semi-crystalline polymers. A good dispersion would result in more crystallization sites during the molding process and further lead to increase the mechanical properties. The presence of the epoxy phase was also noted to possibly have caused the lack of significant improvement in the elastic modulus and flexural properties. During the initial preparation of the virgin polymer, the amine-based triethylenetetramine (TETA) curing agent was utilized. Unlike those polymers synthesized with dynamic covalent bonds, the utilization of the TETA curing agent does not result in a polymer with

reversible chain ends. Thus, in order to rectify this issue, future studies will delve into the utilization or development of a dispersion method for the CNTs as well as introducing dynamic covalent bonds to epoxy phase.

References

[1] Z. Razak, A. Sulong, N. Muhamad, C. Haron, M. Radzi, N. Ismail, D. Tholibon, I. Tharazi. Effects of thermal cycling on physical and tensile properties of injection moulded kenaf/carbon nanotubes/polypropylene hybrid composites. Composites Part B: Engineering 168 (2019) 159–165.

[2] X. Zhang, W. Lu, G. Zhou, Q. Li, Understanding the mechanical and conductive properties of carbon nanotube fibers for smart electronics. Advanced Materials (2019) 1902028.

[3] A.Moumen, M.Tarfaoui, K.Lafdi. Mechanical characterization of carbon nanotubes based polymer composites using indentation tests. Composites PartB: Engineering 114 (2017) 1–7.

[4] F. Meng, H. Wang, F. Huang, Y. Guo, Z. Wang, D. Hui, Z. Zhou. Graphene-based microwave absorbing composites: A review and prospective, Composites Part B: Engineering 137 (2018) 260–277.

[5] M. Mattioli-Belmonte, G. Vozzi, Y. Whulanza, M. Seggiani, V. Fantauzzi, G. Orsini, A. Ahluwalia. Tuning polycaprolactone carbon nanotube composites for bone tissue engineering scaffolds. Materials Science and Engineering: C 32 (2012) 152–159.

[6] F. Gojny, M. Wichmann, U. K¨ opke, B. Fiedler, K. Schulte. Carbon nanotube-reinforced epoxy-composites: enhanced stiffness and fracture toughness at low nanotube content, Composites Science and Technology 64 (2004) 2363–2371.

[7] D. Qian, E. Dickey, R. Andrews, T. Rantell. Load transfer and deformation mechanisms in carbon nanotube polystyrene composites. Applied Physics Letters 76 (2000) 2868–2870.

[8] M. Biercuk, M. Llaguno, M. Radosavljevic, J. Hyun, A. Johnson, J. Fischer. Carbon nanotube composites for thermal management. Applied Physics Letters 80 (2002) 2767–2769.

[9] M. Cadek, J. Coleman, V. Barron, K. Hedicke, W. Blau. Morphological and mechanical properties of carbon nanotube-reinforced semicrystalline and amorphous polymer composites. Applied Physics Letters 81 (2002) 5123–5125.

[10] M.Zakaria, M.Kudus, H.Akil, M.Thirmizir. Comparative study of graphene nanoparticle and multiwall carbon nanotube filled epoxy nanocomposites based on mechanical, thermal and dielectric properties. Composites Part B: Engineering 119 (2017) 57–66.

[11] J. Cha, G. Jun, J. Park, J. Kim, H. Ryu, S. Hong. Improvement of modulus, strength and fracture toughness of cnt/epoxy nanocomposites through the functionalization of carbon nanotubes. Composites Part B: Engineering 129 (2017) 169–179.

[12] M. Kim, Y. Park, O. Okoli, C. Zhang. Processing, characterization, and modeling of carbon nanotube reinforced multiscale composites. Composites Science and Technology 69 (2009) 335–342.

[13] B. Safadi, R. Andrews, E. Grulke. Multiwalled carbon nanotube polymer composites: Synthesis and characterization of thin films. Journal of Applied Polymer Science 84 (2002) 2660–2669.

[14] R. Ansari, M. Aghdam. Micromechanics-based viscoelastic analysis of carbon nanotube-reinforced composites subjected to uniaxial and biaxial loading. Composites Part B: Engineering 90 (2016) 512–522.

[15] M. Yan, L. Liu, L. Chen, N. Li, Y. Jiang, Z. Xu, M. Jing, Y. Hu, L. Liu, X. Zhang. Radiation resistance of carbon fiber-reinforced epoxy composites optimized synergistically by carbon nanotubes in interface area/matrix. Composites Part B: Engineering 172 (2019) 447–457.

[16] R. Haggenmueller, W. Zhou, J. Fischer, K. Winey. Production and characterization of polymer nanocomposites with highly aligned single-walled carbon nanotubes. Journal of Nanoscience and Nanotechnology 3 (2003) 105–110.

[17] P. Potschke, A. Bhattacharyya, A. Janke. Melt mixing of polycarbonate with multiwalled carbon nanotubes: microscopicstudiesonthestateofdispersion. European Polymer Journal 40 (2004) 137–148.

[18] N. Singh, D. Hui, R. Singh, I. Ahuja, L. Feo, F. Fraternali. Recycling of plastic solid wastes: A state of art review and future applications, Composites Part B: Engineering 115 (2017) 409–422.

[19] G. Cicala, E. Pergolizzi, F. Piscopo, D. Carbone, G. Recca. Hybrid composites manufactured by resin infusion370 withafullyrecyclablebioepoxyresin. CompositesPartB:Engineering 132 (2018) 69–76.

[20] G. Karayannidis, D. Achilias. Chemical recycling of poly(ethylene terephthalate). Macromolecular Materials and Engineering 292 (2007) 128–146.

[21] D. Achilias, A. Giannoulis, G. Papageorgiou. Recycling of polymers from plastic packaging materials using the dissolution reprecipitation technique. Polymer Bulletin 63 (2009) 449–465.

[22] A. L. Rosa, D. Banatao, S. Pastine, A. Latteri, G. Cicala. Recycling treatment of carbon fibre/epoxy composites: Materials recovery and characterization and environmental impacts through life cycle assessment. Composites Part B: Engineering 104 (2016) 17–25.

[23] K. Yu, Q. Shi, M. Dunn, T. Wang, H. Qi. Carbon fiber reinforced thermoset composite with near 100% recyclability. Advanced Functional Materials 26 (2016) 6098–6106.

[24] Y. Zhang, A. Broekhuis, F. Picchioni. Thermally self-healing polymeric materials: The next step to recycling thermoset polymers? Macromolecules 42 (2009) 1906–1912.

[25] X. Wang, M. Akobi, P. Nikaeen, A. Khattab, T. He, J. Li, P. Zhang. Modeling and statistical understanding: The effect of carbon nanotube on mechanical properties of recycled polycaprolactone/epoxy composites. Journal of Applied Polymer Science 138 (2021) 49886.

[26] P. Zhang, M. Akobi, A. Khattab. Recyclability/malleability of crack healable polymer composites by response surface methodology. Composites Part B: Engineering 168 (2019) 129–139.

[27] W. Shou, P. Zhang, A. Khattab. Parametric study of an automated nanoparticles spray process for nanofibers/fabric reinforced composites. Polymer Composites 40 (2018) 1068–1077.

[28] P. Zhang, A. Khattab. Characteristics of process-induced properties in carbon nanofibre aqueous dispersion. Micro & Nano Letters 13 (2018) 524–529.

[29] F. Trebuna, E. Ostertagova, P. Frankovsky, O. Ostertag. Application of polynomial regression models in prediction of residual stresses of a transversal beam. American Journal of Mechanical Engineering 4 (2016) 247–251.

[30] S. Dey, S.Naskar, T.Mukhopadhyay, U.Gohs, A.Spickenheuer, L.Bittrich, S. Sriramula, S.Adhikari, G. Heinrich. Uncertain natural frequency analysis of composite plates including effect of noise-a polynomial neural network approach. Composite Structures 143 (2016) 130–142.

[31] C. Li, J. Guo, T. Jiang, X. Zhang, L. Xia, H. Wu, S. Guo, X. Zhang. Extensional flow-induced hybrid crystalline fibrils (shish) in cnt/pla nanocomposite. Carbon 129 (2018) 720–729.

[32] G. Odegard, T. Clancy, T. Gates. Modeling of the mechanical properties of nanoparticle/polymer composites. Polymer 46 (2005) 553–562.

[33] B. Ashrafi, P. Hubert. Modeling the elastic properties of carbon nanotube array/polymer composites. Composites Science and Technology 66 (2006) 387–396.

[34] B. Arash, Q. Wang, V. Varadan. Mechanical properties of carbon nanotube/polymer composites. Scientific Reports 4 (2014) 6479.

[35] S. Kundalwal, V. Choyal. Transversely isotropic elastic properties of carbon nanotubes containing vacancy defects using md. Acta Mechanica 229 (2018) 25712584.

[36] K. Lee, D. Paul. A model for composites containing three-dimensional ellipsoidal inclusions. Polymer 46 (2005) 9064–9080.

[37] K. Yanase,S.Moriyama,J.Ju. Effectsofcntwavinessontheeffectiveelasticresponsesofcnt-reinforcedpolymer composites. Acta Mechanica 224 (2013) 1351–1364.

[38] W. Oliver, G. Phar. An improved technique for determining hardness and elastic modulus using load and displacement sensing indentation experiments. Journal of Materials Research 7 (1992) 1956–1983.

[39] S. S. Asif, K. Wahl, R. Colton. Nanoindentation and contact stiffness measurement using force modulation with a capacitive load-displacement transducer. Review of Scientific Instruments 70 (1999) 1–6.

[40] B. Briscoe, L. Fiori, E. Pelillo. Nano-indentation of polymeric surfaces. Journal of Physics D Applied Physics 31 (1998) 2395–2405.

[41] T. Csan´ adi, D. N´ emeth, C. Zhang, J. Dusza. Nanoindentation derived elastic constants of carbon fibres and their nanostructural based predictions. Carbon 119 (2017) 314–325.

[42] D. Vgenopoulos, J. Sweeney, C. Grant, G. Thompson, P. Spencer, P. Caton-Rose, P. Coates. Nanoindentation analysis of oriented polypropylene: Influence of elastic properties in tension and compression. Polymer 151 (2018) 197–207.

[43] S. Fu, X. Feng, B. Lauke, Y. Mai. Effects of particle size, particle/matrix interface adhesion and particle loading on mechanical properties of particulate-polymer composites. Composites Part B: Engineering 39 (2008) 933– 961.